Cellulose (2020) 27:9227–9241
https://doi.org/10.1007/s10570-020-03438-6

ORIGINAL RESEARCH

Tailoring of rheological properties and structural polydispersity effects in microfibrillated cellulose suspensions

Goksu Cinar Ciftci · Per A. Larsson · Anastasia V. Riazanova · Hans Henrik Øvrebø · Lars Wågberg · Lars A. Berglund

Received: 28 April 2020 / Accepted: 3 September 2020 / Published online: 16 September 2020

Abstract Industrial production of low-charge microfibrillated cellulose (MFC) typically results in wide fibril size distributions. This polydispersity influences viscosity, overall colloidal stability, and rheological properties of MFC suspensions and gels in aqueous systems. In this work, a systematic rheological analysis is performed for industrially prepared MFC and fractions of different size distributions. Gel formation and flow characteristics (e.g., shear-thinning) of each fraction are examined under neutral and acidic conditions and compared with the unfractionated MFC suspension. The effects of size, aspect ratio, and surface charge on the rheology of semi-dilute MFC suspensions are discussed. The results demonstrate that particle size and aspect ratio distribution control the viscoelasticity and shear-thinning properties of MFC suspensions. An increased fraction of small diameter nanofibrils, by ex situ addition of the fine particles with high aspect ratio or removal of the coarsest particles (with lower aspect ratio) by fractionation, significantly enhances the storage modulus and the yield stress of the complex mixture, compared to the properties of the coarser fractions. New insights are also reported on the tailoring of the rheology of highly polydisperse fibrillar mixtures, where the rheological contributions of each fraction are discussed.

Electronic supplementary material The online version of this article (https://doi.org/10.1007/s10570-020-03438-6) contains supplementary material, which is available to authorized users.

G. Cinar Ciftci (✉) · P. A. Larsson · A. V. Riazanova · L. Wågberg · L. A. Berglund
Department of Fibre and Polymer Technology, KTH Royal Institute of Technology, Stockholm, Sweden
e-mail: goksucc@kth.se

H. H. Øvrebø
Borregaard AS, Sarpsborg, Norway

Graphic abstract

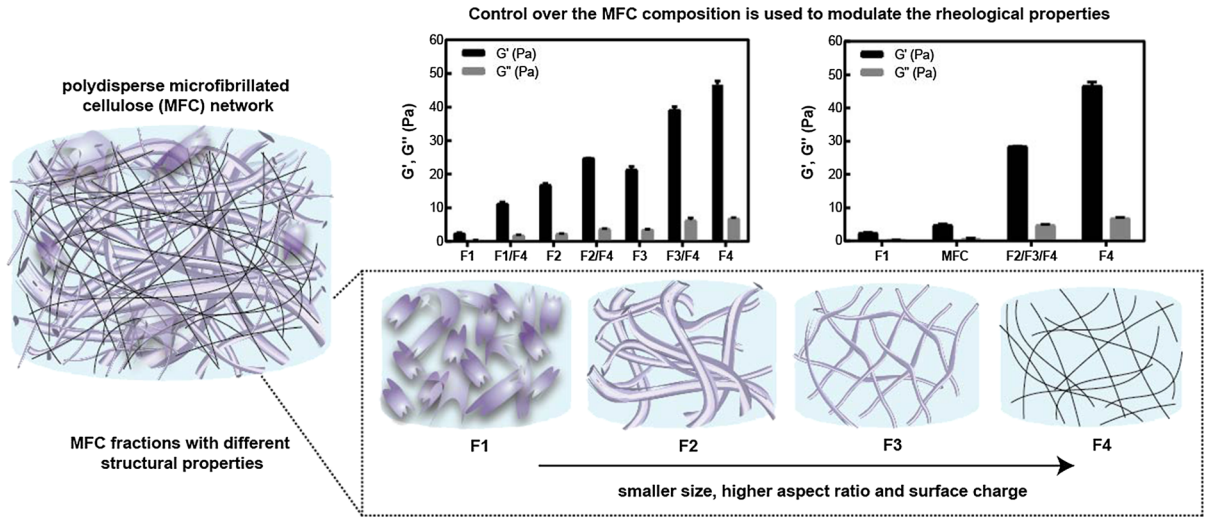

Keywords Nanocellulose · Cellulose nanofibrils · Viscoelasticity · Gel formation · Shear-thinning

Introduction

Plants are sustainable sources of advanced materials, with the ability to provide us greener alternatives to today's commercially available petrochemical-based products. Cellulosic materials with their exceptional physical and mechanical properties have been used for textiles, construction materials, and papermaking for centuries (Hon 1994). The disintegration of cellulose fibres, with different combinations of pre- and post-treatment, has led to the development of cellulose nanomaterials, such as cellulose nanofibrils (CNF; also called nanofibrillated cellulose, NFC) and microfibrillated cellulose (MFC). These cellulose nanomaterials have a large specific surface area, semi-crystalline order, and a variety of functionalities (Kargarzadeh et al. 2018). Cellulose nanomaterials and their composites show promise in applications such as fibre reinforced composites, adhesives and coatings, emulsions and cosmetics, packaging, electronics, and sensors (Thomas et al. 2018). These diverse applications have roots in the structural properties of differently produced MFC and CNF. Properties such as size, length, aspect ratio, and surface charge depend on the source of the cellulose raw material and manufacturing conditions (Siqueira et al. 2010; Nechyporchuk et al. 2016a). In general, MFC consists of coarser particles and bundles of cellulose nanofibrils, having a relatively low charge, and a broad size distribution ranging from micro- to nanometres in diameter (Osong et al. 2016; Dimic-Misic et al. 2018; Larsson et al. 2019) in contrast to the more homogeneous CNF produced from fibres that are chemically pre-treated to control charge properties (Isogai 2013; Fall et al. 2011).

MFC and CNF can form highly entangled fibrillar networks in water, with a predominantly elastic response, i.e., the storage modulus (G') exceeds the loss modulus (G''), even at low solids contents (Pääkkö et al. 2007). The mechanism of fibrillar network formation was first proposed by Mason (1954) based on a mechanical entanglement model in which the contact points between the fibres contribute to the network strength of a wet fibrous system. This phenomenon has been thoroughly examined with the definition of an entanglement threshold or crowding factor (N), which depends on the concentration and aspect ratio of the monodisperse particles (Kerekes and Schell 1992). The concept has also been expanded by introducing connectivity and rigidity thresholds based on percolation and effective medium theories (Celzard et al. 2008, 2009) and was recently used to characterize the gelation mechanism and flow properties of highly charged CNF in aqueous suspensions (Geng et al. 2018). The viscosity and

storage moduli of the CNF suspensions decreased with increasing charge density due to lower aggregation tendency and crowding factor at the same concentration (Geng et al. 2018). In addition to this, it has been shown that the gel strength and network formation propensity could be increased by the electrostatic screening or neutralization of the surface charges, either by increased ionic strength or a reduced pH of semi-dilute CNF suspensions (Fall et al. 2013; Saito et al. 2011; Fall et al. 2011).

Flow characteristics of MFC and CNF suspensions, and the shear-induced organization of the network have also been investigated for processing and rheology modification (Hubbe et al. 2017). In particular, the anisotropic nature of MFC and CNF contributes to hydrodynamic alignment and disentanglement of the components when subjected to shear forces. Reorganization of the fibrous network leads to a decreased viscosity with increasing shear rate and results in a shear-thinning effect. Moreover, the addition of MFC as a rheology modifier enhances shear-thinning flow behaviour and colloidal stability of aqueous systems. For example, MFC-containing adhesive was more uniformly distributed in the particle board due to the shear-thinning nature of the mixture (Mahrdt et al. 2016). In addition, the presence of MFC in coloured coating formulations resulted in less flocculation of the dye particles (Dimic-Misic et al. 2013; Oh et al. 2017). The intrinsic viscoelastic properties and flow characteristics of MFC suspensions widen their use as rheology modifiers, ultimately increasing the number of commercial applications (Nechyporchuk et al. 2016a).

The demand for MFC in industrial applications has paved the way for production in a more substantial, commercial scale. Such materials consist of both micro- and nanofibrillated particles with brush-like fibril morphology (Holtan et al. 2019; Larsson et al. 2019). It is also likely that commercially available MFC grades, at least low-charged ones, show a more heterogeneous architecture in terms of size distribution than laboratory-made grades. This represents challenges not only to fundamental structural characterizations but also to rheological fingerprinting of the material for processing (Larsson et al. 2019; Desmaisons et al. 2017). Structural polydispersity can be tuned, either by controlling the degree of fibrillation or by optimizing the size distribution via addition or separation of the constituents after the processing. One distinct approach for controlling the state of suspension is to alter the number of homogenization/microfluidization steps, in order to control the degree of fibrillation and resultant rheological properties (Taheri and Samyn 2016). In a recent study by Schenker et al. (2019), mixtures of different fibres and fibrils with broad size distributions were examined. It was shown that the coexistence of macro-scale residual fibre and nanofibrillated particles had a significant impact on the rheological behaviour of polydisperse MFC suspensions.

In this work, an important objective was to find conditions and characterization protocols that can be used to analyse the impact of MFC fractions on the resulting rheological properties. Such methodologies could then be used for quality control of industrial MFC grades. Furthermore, in many applications of MFC, only low-concentration (i.e., lower than 0.5 wt%) mixtures are used (coatings, paints, adhesives, or personal care products), where performance is dictated by suspension rheology. Hence, a fundamental understanding of how MFC polydispersity influences rheology is therefore essential in the development of new MFC products.

No studies on the rheology of different MFC fractions could be found in previous literature. The first part of the present work was devoted to characterizing the gel network and flow properties of a commercial MFC, and fractions containing microfibrils of different sizes. Self-recovery of the polydisperse MFC gel was also examined to relate these properties to the rheology of more monodisperse CNF gels. Gel formation and shear-thinning phenomena were also analysed at different solid contents. To reveal the impact of structural polydispersity on the rheology, the commercial MFC was fractionated, and the fractionated suspensions were prepared slightly above the gel formation threshold (i.e., when $G' > G''$). A systematic analysis of the suspensions from each fraction was used to establish a basic understanding of the effects of size, aspect ratio, and surface charge distribution of the individual particles. Finally, a tuning of rheological properties was accomplished by controlling fraction sizes in the polydisperse MFC mixture.

Materials and methods

Materials

In this study, a commercial 1.9 wt% MFC, produced by Borregaard AS (Sarpsborg, Norway) from a bleached sulphite pulp, was used without any further chemical modification or treatment after it was received. For the preparation of more dilute MFC suspensions, the stock grade was diluted using deionized water, and homogenized by a mixer.

Fractionation of the MFC

A volume of 0.5 l of the MFC suspension (0.2 wt%) was fractionated into four different size fractions according to a recently developed protocol (Larsson et al. 2019), that combines sequential filtrations with a final centrifugation step. For the separation of the two coarsest fractions (F1 and F2), a screen with a 20 μm pore size (Paper Research Material Inc., U.S.) and a Twilled Dutch 325 × 2300 metal mesh with a nominal filter rating of 1–2 μm (G. Bopp & Co AG, Zürich, Switzerland) were used as the screens in a Britt Dynamic Drainage Jar. The filtrate passing the fine mesh was then separated into two fractions (F3 and F4) by centrifugation at 4500 rpm for 1 h. The colloidally stable supernatant F4 and the sedimented F3 were collected separately.

After the fractionation, the concentrations of F1, F2, F3, and F4 suspensions were determined gravimetrically to be 0.14, 0.08, 0.39, and 0.01 wt %, respectively. The F1, F2, and F4 fractions were concentrated to 0.4 wt%, i.e., the same consistency as F3, via sedimentation (for F1 and F2) or rotary evaporation at 70 °C under vacuum (for F4). F1/F4, F2/F4 and F3/F4 suspensions were prepared by mixing F4 suspension (at 0.4 wt%) with F1, F2 or F3 suspensions (at 0.4 wt%) to have a 50:50 weight mixing ratios. In addition, the first step of the fractionation was performed using a screen with a 20 μm pore size to obtain the mixture of F2/F3/F4 suspension, and the concentration of the filtrate (F2/F3/F4) was adjusted to 0.4 wt%.

Characterization of MFC morphology and surface charge

Morphology was studied using a Hitachi S-4800 field-emission Scanning Electron Microscope (SEM) for high-resolution imaging, and a Hitachi TM-1000 Tabletop SEM for low magnification. Samples were prepared by vacuum filtration of very dilute MFC fractions through a nanoporous aluminium oxide membrane (FlexiPor 20 nm; SmartMembranes GmbH, Halle, Germany), and were coated with a thin layer of platinum–palladium to prevent charging artifacts during the imaging. For each MFC fraction, seven to nine different SEM micrographs were analysed to determine the length, width and aspect ratio distributions (Fig. S3).

The surface charge of each sample was determined by polyelectrolyte titration with the aid of a Stabino particle charge titrator (Particle Metrix Gmbh, Meerbusch, Germany), using 400–500 kDa poly(diallyldimethylammonium chloride) (PDADMAC) as a titrant, with different concentrations corresponding to a charge of 0.347 μmol/ml for the unfractionated MFC, and 0.0267 μmol/ml for the fractionated samples.

Rheological characterizations

The rheological analysis of the samples was carried out in a DHR-2 rheometer (TA Instruments, New Castle, DE, USA) equipped with a plate–plate geometry with a diameter of 25 mm (1 mm gap distance) and a Peltier system for temperature control the temperature at 25 °C, and a solvent trap to prevent evaporation. Each sample was allowed to equilibrate for 10 min before the analysis. To characterize the linear viscoelastic (LVE) regime of the MFC (1.9 wt%), strain (γ) and frequency (ω) sweep analyses were conducted in the strain range of 0.06–100% and frequency range of 1–100 rad/s, respectively. Time sweep tests were performed at constant strain (0.1%) and frequency (10 rad/s) to determine the equilibrium elastic moduli of the samples in the LVE regime. Flow analysis were performed between 0.01 and 1000 s^{-1} for the MFC suspensions at different concentrations (1.9, 1, 0.5, 0.4, 0.2 and 0.1 wt%) and the suspensions of each fraction at 0.4 wt%. Flow curves were obtained with automated acquisition time

mode and shear-rate control provided by the DHR-2 rheometer to prevent flow-instabilities.

To characterize linear viscoelastic and flow properties of the MFC and the suspensions of each fraction (0.4 wt%) under acidic conditions (pH $\sim$ 2), a small amount of concentrated HCl was injected into the sample through a syringe (Fall et al. 2013). After the injection, time-sweep analysis at constant strain (0.1%) and frequency (10 rad/s) were immediately initiated and continued for 1 h to reach equilibrium conditions. Then, the flow analysis of the samples was performed between 0.01 and 1000 s^{-1}, and the yield stresses were estimated using the Herschel–Bulkley equation above 20 s^{-1} (Eq. 1) (Karppinen et al. 2011).

The rheological properties of the mixtures of different MFC fractions were analysed under the same experimental conditions. First, the equilibrium moduli of the mixtures (0.4 wt%) were determined at 0.1% strain and 10 rad/s frequency, then, flow analysis was performed between 0.1 and 1000 s^{-1} to examine shear-thinning behaviour and estimate yield stresses of the mixtures. All rheological measurements were performed at least in triplicates. The results were given as an average of the independent measurements with standard deviations.

Results and discussion

Structural properties of commercial MFC

The rheology of MFC suspensions is expected to depend on MFC morphology such as size, shape, and aspect ratio of the constitutes. Recently, we developed a fractionation approach to characterize size and surface charge distribution in commercial MFC grades (Larsson et al. 2019). In this approach, the *coarsest* (F1) and *coarse* (F2) fractions were collected by sequential filtration, and then centrifugation was carried out to separate *fine* (F3), and *finest* (F4) constituents (Fig. S1). The fibril length and width distributions of polydisperse MFC were quantified from SEM micrographs and the use of image processing (ImageJ) to estimate the average particle aspect ratios in each fraction (Table S1 and Fig. S3). As seen in Fig. 1 and Table 1, the coarsest fraction (F1), constituting 7.3% of the total mass, consists of low-aspect-ratio ($\approx$ 11) micrometre-sized fibre fragments. Higher aspect-ratio branched fibrils with a gradually decreasing width were observed in the finer fractions (F2 to F4). These fibrils have not been fully fibrillated, and this is the reason for the branched structure.

In addition to structural assessment, the surface charge was determined using polyelectrolyte titration since surface charge plays a critical role in network formation and rheological characteristics of the cellulosic suspensions. As listed in Table 1, the surface charge increased with decreasing MFC fibril size. Although the present MFC grade has a highly complex and polydisperse architecture (Fig. 1), the mass fraction distribution in the system was dominated by the two finer and more highly charged nanofibrillated fractions: F3 and F4. Note that the "missing" fraction of 17%, termed "Lost material" at the bottom of Table 1, is dominated by a fine fraction of nanofibrils (Larsson et al. 2019). Consequently, as much as 38% of the total MFC population (F4 + Lost material) could be in the form of fine fibrils with a diameter of less than 100 nm.

Viscoelasticity and flow properties

Rheological properties of the unfractionated, non-diluted MFC suspension at 1.9 wt% (Fig. 2a) were studied to determine the LVE regime at different amplitudes and frequencies (Fig. S2). The critical strain (γ_c) of the network was determined about 3% at 10 rad/s from the intersection of the two lines plotted in Fig. S2 which show the onset for the destruction of the network (Swerin et al. 1992), and the commercial MFC was less sensitive to the frequency changes in the range of 1–100 rad/s at constant strain (0.1%) (Fig. S2). In the LVE regime, the polydisperse MFC formed a fibrillar gel network (i.e., when $G' > G''$), and the equilibrium modulus was determined to be $\sim$ 1.7 kPa (Fig. 2b). This value is of the same magnitude as a 2 wt% CNF gel ($G' \approx 10^3$ Pa) with a particle width in the 5–20 nm range (Pääkkö et al. 2007).

When the flow properties were examined by continuous shearing in the range of low to high shear rates (0.01–1000 s^{-1}), a shear-thinning flow profile was observed (Fig. 2c), which is typical for anisotropic CNF gels (Nechyporchuk et al. 2016b). Under low shear rate, the material displayed high viscosity, owing to a physically entangled fibrillar network. In contrast, an increased shear rate resulted in a significantly decreased viscosity due to the structural

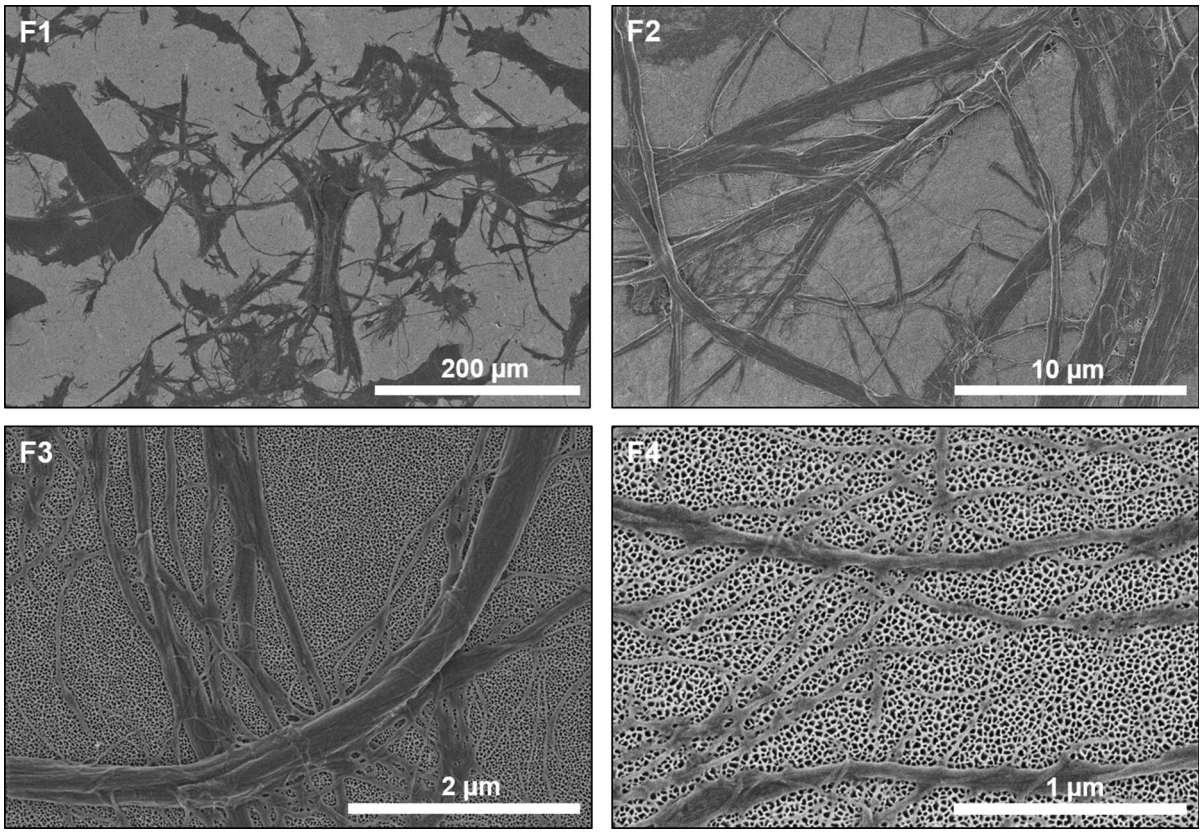

Fig. 1 SEM micrographs of the MFC fractions F1, F2, F3 and F4 used for the rheological analysis

Table 1 Structural properties of the MFC fractions and the commercial, unfractionated MFC

	Particle width	Aspect ratio	Surface charge (µmol/g)	Mass fraction (%)[a]
F1 (coarsest)	5–50 µm	11 ± 7	N.A.[b]	7.3 ± 0.6
F2 (coarse)	200 nm–1 µm	44 ± 24	3.4 ± 0.2	13.3 ± 2.5
F3 (fine)	100–300 nm	51 ± 23	17.1 ± 0.7	42.6 ± 2.9
F4 (finest)	20–100 nm	78 ± 18	43.5 ± 1.9	21.0 ± 1.3
MFC (unfractionated)	20 nm–50 µm		39.5 ± 2.2	

[a]Lost material was determined as 17 ± 0.4% of the total mass after fractionation and consisted mainly of F3 and F4 fractions (Larsson et al. 2019)

[b]The surface charge was too low to be measured by polyelectrolyte titration

reorganization and disentanglement of the MFC particles.

The self-recovery properties of the 1.9 wt% MFC gel were also examined by cyclic transitions from the linear small-strain region to the non-linear large-strain viscoelastic regime ($\gamma > \gamma_c$). The MFC network returned to its original gel state repetitively whenever the strain amplitude was reduced ($\gamma < \gamma_c$) (Fig. 2d). It is therefore suggested that there is a dynamic network formation within the MFC system as a result of reversible non-covalent interactions between the MFC components. It is also expected that branched physical entanglements are important for the remarkable elastic recovery, even at large deformation. Despite the highly polydisperse structural properties of the MFC (Table 1), the observed self-recovery of the 1.9 wt%

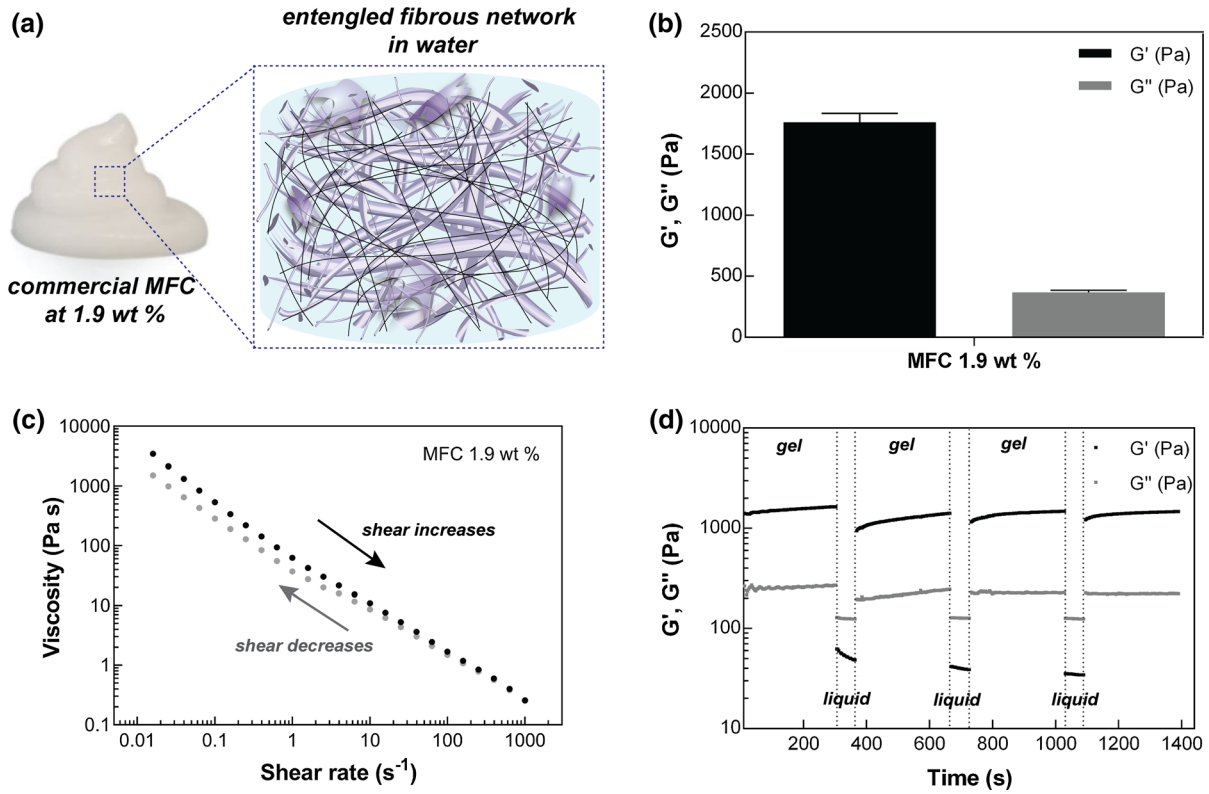

Fig. 2 **a** Photo and schematic representation of an unfractionated MFC at a solids content of 1.9 wt% showing **b** gel-like properties ($G' > G''$), with typical flow behaviour such as **c** shear thinning and **d** self-recovery of gel properties at 0.1% strain after large-strain deformation at 50%

MFC gel was comparable to that of a 1 wt% TEMPO-oxidised monodisperse CNF gel (Mendoza et al. 2018). It is hence likely that the finest fractions, such as F4 in this work, are important for the self-recovery of the gel network.

In the work of Hill (2008), low and high concentration gels of MFC were studied in the LVE regime. It was shown that bulk elastic moduli were independent of the structural polydispersity when MFC network components have a large enough aspect ratio to form an interconnected fibrous network. From Table 1, it is clear that the high-aspect-ratio fibrils in the finer fractions can readily form a highly entangled network, and this occurs even in the presence of coarser, low-aspect-ratio fibrils. Since we aim to explore the effect of MFC dimensions/aspect ratio on rheology, concentrations as high as 1.9% would not be very sensitive to effects from different fractions.

The effects of MFC concentration on network formation and flow characteristics were investigated in order to find the critical concentration for gelation where storage modulus is higher than loss modulus. As shown in Fig. 3a, the MFC suspension showed gel-like behaviour above 0.1 wt% ($G' > G''$). Above this consistency, G' increased exponentially as a function of concentration (Fig. 3b). Fitting a power-law relation to the storage moduli data ($G' \sim c^{\alpha}$) yielded $\alpha = 4.1$, which is in the range between 3.7 and 7, as proposed by Hill (2008) for MFC networks at low and high volume fractions, respectively (Fig. 3b).

The shear viscosity profiles of MFC suspensions were also analysed as a function of concentration and shear rate. Higher viscosities were observed at low shear rates (Fig. 4a), and at higher shear rates, the MFC fibrils started to orient along the direction of shear, leading to decreased viscosity. However, with increasing MFC concentration, the viscosity decreased more strongly with increasing shear rate, and large deviations from a Newtonian flow behaviour were observed above 0.1 wt% (Fig. 4a).

The concentration-dependent flow properties were quantified by fitting the results to the power-law

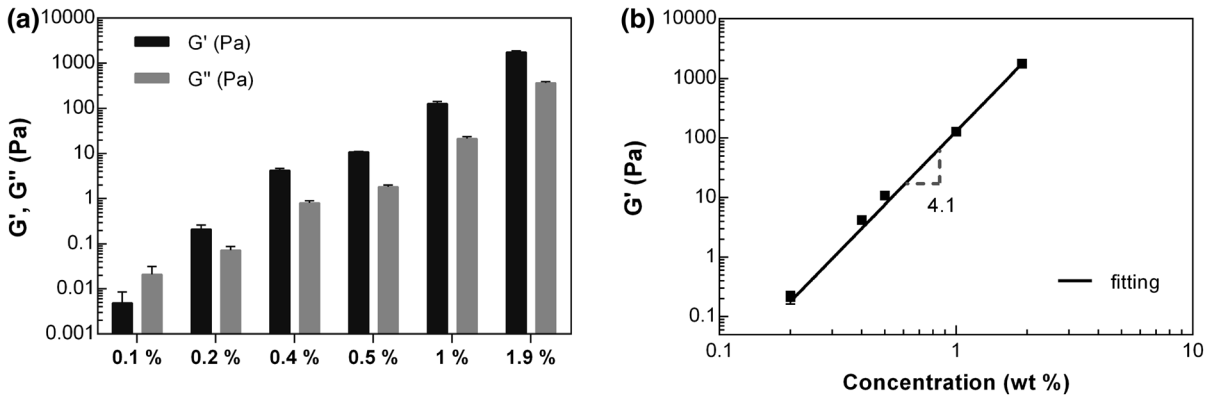

Fig. 3 Concentration-dependency for **a** the equilibrium storage and loss moduli of unfractionated MFC suspensions at constant strain (0.1%) and frequency (10 rad/s), **b** the power-law fit to the storage moduli of the suspensions

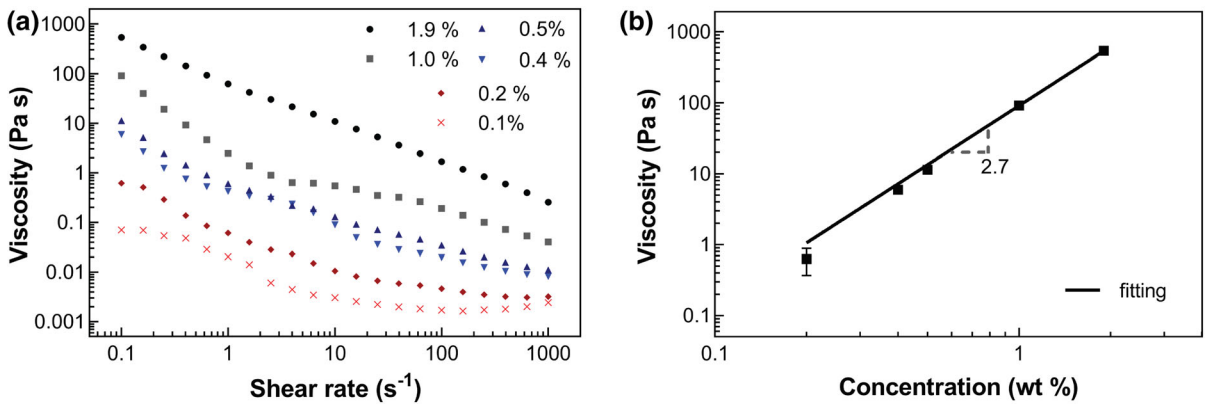

Fig. 4 **a** Viscosity profiles of the unfractionated MFC suspensions at different concentrations over a shear rate ranging from 0.1 to 1000 s^{-1}, and **b** concentration-dependent viscosities at a constant shear rate of 0.1 s^{-1}

relationship (*viscosity* $\sim c^{\beta}$). The shear viscosity values were found to scale exponentially with the concentration to the power of 2.7, at a shear rate of 0.1 s^{-1} (Fig. 4b). In this work, the fitted exponent was slightly higher than the values reported by Naderi et al. (2014), but this is most likely related to differences in MFC fibrillar structure and properties, and experimental conditions (Lasseuguette et al. 2008). Moreover, the present storage modulus was much more sensitive to concentration changes than the shear viscosity, resulting in a higher exponent (compare Figs. 3b, 4b).

Viscoelastic properties of different MFC fractions

Suspensions of the fractionated MFC were prepared at 0.4 wt% because this is a suitable semi-dilute concentration for gel network formation (Fig. 3), showing shear-thinning flow behaviour in a broad range of shear rates (Fig. 4). At this concentration, it is also expected that small differences in MFC fibril shape, size, and charge would affect the rheological behaviour.

Time sweep analyses were carried out at constant strain (0.1%) and frequency (10 rad/s) in the range of linear viscoelastic regime (Fig. S4). As shown in Fig. 5, all fractions showed a gel-like viscoelastic response ($G' > G''$), and G' was strongly increased as the fibril dimensions were decreased. The F4 network, constituted of high-aspect-ratio nanofibrils, showed the highest values for G' (Fig. 5). On the other hand, the F1 suspension with low aspect-ratio fibre fragments had the lowest storage modulus, even lower than G' for the unfractionated commercial MFC grade (Fig. 5). This data shows that the viscoelasticity of the

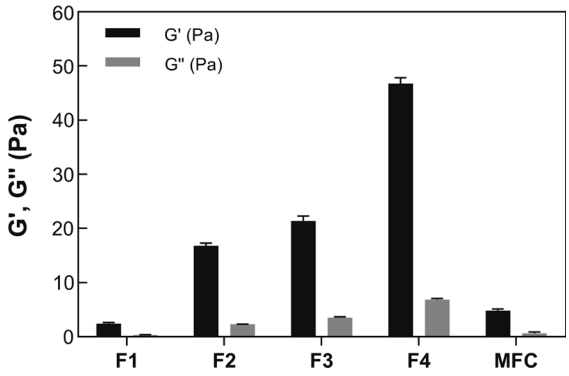

Fig. 5 Equilibrium storage (G′) and loss moduli (G″) of 0.4 wt% MFC fractions and unfractionated MFC at constant frequency (10 rad/s) and strain (0.1%)

polydisperse MFC network is strongly influenced by the size and aspect ratio of the microfibrils.

Flow properties and yield stress of the different MFC fractions

The shear-thinning behaviour of the fractions was investigated at a concentration of 0.4%, i.e., in a region where they all form gels. Although all fractions exhibited shear-thinning, the coarsest F1 fraction displayed a deviating behaviour where no further shear-thinning was observed at shear rates greater than 20 s^{-1} (Fig. 6a). Interestingly, the viscosities of the F2, F3, and unfractionated MFC suspensions were of the same order of magnitude at high shear rates ($> 20\ s^{-1}$), whereas the finest fraction (F4) had a slightly higher viscosity. The significantly lower aspect ratio of F1 is probably the reason for the distinct viscosity profile, as also suggested by Tanaka et al. (2015). The intrinsic viscosity of nanocellulose suspensions is likely to correlate with the aspect ratio of the constituting fibrils. Besides, an increased aspect ratio results in higher viscosity, due to stronger hydrodynamic interactions between the fibrils (Tanaka et al. 2015; Switzer and Klingenberg 2003). To investigate this relationship, the viscosities of the fractions were plotted as a function of the average aspect ratios of each fraction (Table 1). As shown in Fig. 6b, the viscosities increased proportionally with the fibril aspect ratio.

The typical flow curve of an MFC suspension consists of a transition region (i.e., between 0.1 and 10 s^{-1}) before the high shear zone in which the viscosity profile follows a power-law relation (Schenker et al. 2018). The transition region in the viscosity profile was suggested to occur due to the structural reorganization and physical entanglements of the network components, which resulted in temporary inhomogeneities in the flow characteristics (Karppinen et al. 2012). As seen in Fig. 4a, this transition behaviour was highly dependent on the solid contents (Schenker et al. 2018), and also structural properties of the MFC fractions (Fig. 6a). Interestingly, the transition in the viscosity profile of F1 was much more apparent compared to the viscosity profiles of the finer fractions (F2–F4) between 0.1 and 10 s^{-1} (indicated by an arrow in Fig. 6a). This phenomenon can be in-depth investigated using imaging techniques such as optical coherence tomography (Lauri et al. 2017; Koponen et al. 2018) to visualize and quantify apparent fluctuations in rheological properties of the MFC fractions under flow.

Increased network interactions for flexible, high-aspect-ratio fibrils may also be in the form of physical entanglements. The yield stress of the MFC network should then increase which under certain conditions would make MFC fibrils good stabilizers for dispersions or emulsions. In complex industrial products such as paints and coatings, this may hinder the sedimentation of large additives in particle form. For estimation of the apparent yield stress (τ_0) of each fraction, the shear stress (τ) versus shear rate ($\dot{\gamma}$) data above 20 s^{-1} (Fig. 6c) were fitted to the Herschel–Bulkley equation (Eq. 1) (Karppinen et al. 2011), where k is a consistency index, and n is a flow behaviour index ($n < 1$ for shear-thinning fluids, $n = 1$ for Newtonian fluids, and $n > 1$ for shear-thickening fluids).

$$\tau = \tau_0 + k\,(\dot{\gamma})^n \quad (1)$$

The Herschel–Bulkey model, a simple power-law relation given in Eq. 1, describes the flow behaviour of non-Newtonian fluids (Mullineux 2008), and it has been successfully used for the calculations of the apparent yield stress of different MFC suspensions (Koponen 2020; Mohtaschemi et al. 2014; Kumar et al. 2016; Song et al. 2019). On the other hand, the Herschel-Bulkley model does not apply very well to the transition region of the flow curves, which was apparent at shear rates between 0.1 and 10 s^{-1} (Figs. 6a, 7c and 9a). For this reason, the yield stresses

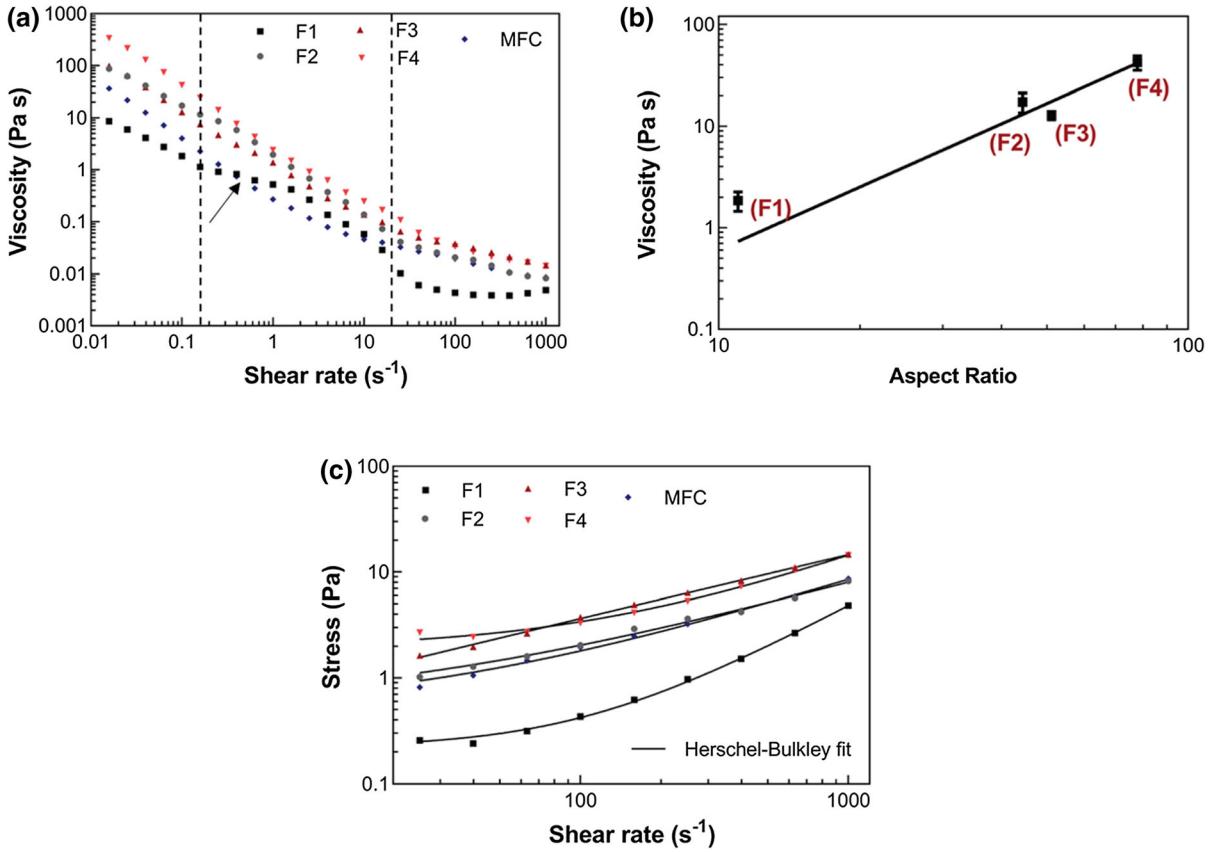

Fig. 6 Flow properties of the 0.4 wt% MFC fractions and unfractionated MFC; **a** viscosity as a function of shear rate (the dashed lines between 0.1 and 20 s^{-1} indicate the transition region) **b** viscosity at 0.1 s^{-1} as a function of aspect ratio, and **c** shear stress as a function of shear rate with the Herschel–Bulkley model fits

were estimated using the model above 20 s^{-1}, following the same approach described by the previous studies (Karppinen et al. 2011; Taheri and Samyn 2016; Dimic-Misic et al. 2013). It is important to note that yield stress of MFC suspensions can also be determined by viscoelastic measurements (Swerin et al. 1992; Hubbe et al. 2017), and the obtained values can be dependent on the fitted model, methodology and measuring geometry. Therefore, the yield stresses of the fraction suspensions were comparable rather than their absolute material characteristics (Karppinen et al. 2011).

As shown in Table 2, the yield stresses of the suspensions were significantly increased by a decreased MFC fibril size, from the low-aspect-ratio F1 to the finer fractions F2, F3, F4 containing higher-aspect-ratio fibrils. Also, the viscosity profile of F1 at high shear-rates (Fig. 6a) was significantly different from the other three high aspect ratio fractions (Tanaka et al. 2015). The flow index of the F1 fraction was greater than unity above 20 s^{-1}.

Effect of surface charges and pH on the rheology of the different MFC fractions

The fibrils in the coarsest fraction (F1) have a very low surface charge, whereas the finer fractions have higher surface charge, ranging from ∼ 3.4 to ∼ 43.5 µmol/g (Table 1). Rheological measurements were also conducted to assess the influence of charge on the gel formation and flow characteristics of each fraction by reducing the pH (Fall et al. 2013). In contrast to a neutral or higher pH where the MFC particles will be charged, a decreased pH results in protonation of carboxyl groups. This protonation eliminates the repulsive Coulombic interactions and contributes to the formation of a purely physically entangled gel network (Fall et al. 2013).

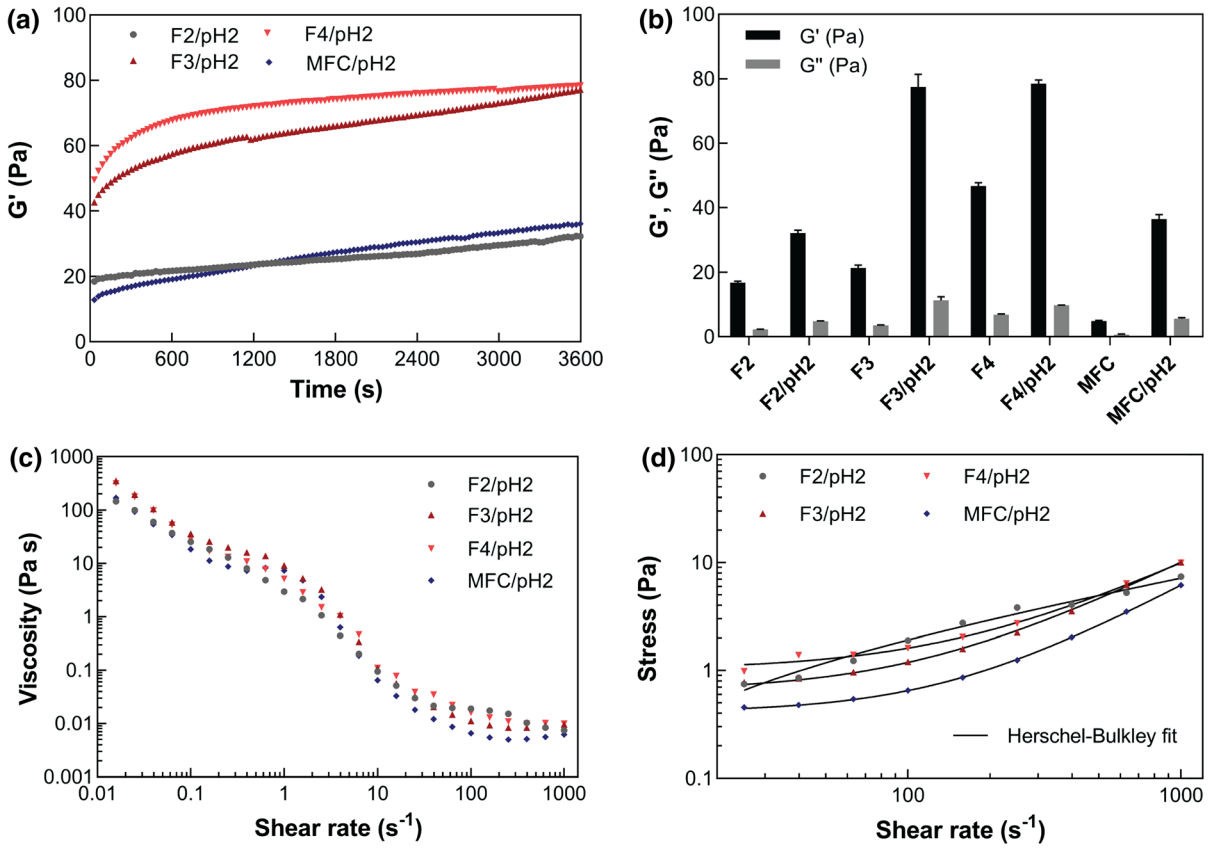

Fig. 7 Linear viscoelastic and flow properties of 0.4 wt% suspensions of fractionated and unfractionated MFC at pH 2; **a** storage modulus as a function of time after injection of acid, **b** comparison of storage and loss moduli with those under neutral conditions, **c** viscosity and **d** shear stress as a function of shear rate with the Herschel–Bulkley model fits

Table 2 Calculated yield stress and flow index (n) at neutral pH according to the Herschel–Bulkley model

	Yield stress (Pa)	n	R^2
F1 (coarsest)	0.2 ± 0.1	1.4	0.99
F2 (coarse)	0.6 ± 0.1	0.7	0.99
F3 (fine)	0.8 ± 0.2	0.7	0.99
F4 (finest)	1.7 ± 0.3	0.9	0.99
MFC (unfractionated)	0.4 ± 0.1	0.8	0.99

The storage modulus of all samples increased as a function of time after acid injection due to larger fibril entanglements once the repulsive interactions between the fibrils were removed (Fig. 7a, b). It could also be detected that the highly charged suspensions, i.e., F3 and F4, responded more rapidly to the pH change and showed a faster increase in storage modulus over the first 10 min (Fig. 7a). On the other hand, the behaviour of the unfractionated MFC is interesting. Although the surface charge ($\sim$ 39.5 µmol/g) is close to that of the finest fraction F4 ($\sim$ 43.5 µmol/g), the increase in G′ was significantly slower than for the finer fractions. Indeed, the two coarsest fractions do only represent $\sim$ 20% of the total MFC mass, these fractions likely control the viscoelastic properties of unfractionated MFC, leading to a slower response to the injection of acid.

Under acidic conditions, all samples displayed a shear-thinning viscosity profile between 0.01 and 20 s^{-1} (Fig. 7c). On the other hand, the shear-thinning of the suspensions became less pronounced above 20 s^{-1} compared to the viscosity profile at neutral pH (Fig. 6a). This result might be explained by increasing fibril–fibril interactions and more extensive entanglements at acidic pH (as also noticed as G' increase),

resulting in reduce fibril orientation and a lowered shear-thinning under high shear rates.

Yield stress and flow index of the suspensions at acidic pH were also estimated using the Herschel–Bulkley model. The shear stress versus shear rate data (Fig. 7d) was fitted to this relation (Eq. 1). As shown in Table 3, the yield stress of the fractions increased as the size of the fractions decreased at acidic pH. When the flow indices of the suspensions were compared, only the low-charged F2 fraction had the flow index lower than unity above 20 s^{-1} (n = 0.6) and was relatively insensitive to the lowering in pH (Tables 2 and 3).

Tailoring of the viscoelastic and flow properties by controlling the MFC composition

The structural polydispersity can be tuned, either by controlling the degree of fibrillation or by optimizing the size distribution via addition or separation of the constituents after processing. Mixtures of MFC fractions (1:1 w/w) were prepared by the addition of the finest fraction (F4) to modulate the gel and flow properties of coarser suspensions (Table S2). As shown in Fig. 8a, the addition of F4 resulted in higher storage moduli for F1/F4, F2/F4, and F3/F4 suspensions compared to the neat F1, F2, and F3 networks, all at the same consistency. Although the F4 fraction has a much higher surface charge which could lead to higher repulsion between the components and less physical entanglement in the network, the results suggest that the decrease in average fibril size is more determinant on the viscoelastic property of polydisperse MFC mixtures at neutral condition (Fig. 8a).

Another route towards optimized MFC fibril distribution is to remove the low-aspect-ratio coarsest particles. To achieve this, only the first step of the fractionation protocol was carried out, and the filtrate was collected as a mixture of finer fractions (F2/F3/F4). It is important to note that "Lost material" (Table 1), remained in the mixture for this procedure. Similarly to the addition of F4 fibrils, the removal of F1 increased the storage modulus significantly (Fig. 8b). For instance, G' increased from ~ 5 Pa for MFC to ~ 30 MPa for F2/F3/F4.

The flow characteristics of the fraction mixtures were also examined at a concentration of 0.4 wt%, and all suspensions displayed shear-thinning viscosity profiles (Fig. 9a). As shown in Fig. 9 and Table 4, the viscosity and yield stress of the MFC compositions can be increased either through the addition of finer fibrils to coarser fractions or through the removal of the coarser particles from a polydisperse MFC grade.

Table 3 Yield stress and flow index based on the Herschel-Bulkley model at acidic pH

	Yield stress (Pa)	n	R^2
F2 (coarse)	0.2 ± 0.1	0.6	0.98
F3 (fine)	0.8 ± 0.2	1.3	0.99
F4 (finest)	0.9 ± 0.2	1.2	0.99
MFC (unfractionated)	0.4 ± 0.1	1.4	0.99

Conclusions

The rheological properties of a commercial MFC were systematically analysed to understand the structure-viscoelasticity relationship of polydisperse networks. Furthermore, it was shown how control over the microfibril size distribution could be used to modulate the rheological performance of a MFC suspension. Despite the notable heterogeneity, the MFC exhibited remarkable viscoelastic properties and interesting gel recovery behaviour similar to that of monodisperse CNF gels. Power-law relationships were fitted to the concentration-dependent viscoelastic and flow properties, and the exponents for both storage modulus and viscosity were found to be in the same range as those of comparable nanocellulose gels.

The distinct behavior of fractions with different microfibril size distribution is important for tailoring of the rheological properties. Storage modulus, viscosity and yield stress all increased substantially as the average microfibril size was decreased. As charge interaction was removed by lowered pH, physical entanglements became more important, and the storage modulus rapidly increased for the two finest fractions with higher surface charges.

The presence of coarser, low-aspect-ratio particles (in this study, the coarsest particles constituted 7.3% of the total mass) significantly affected the rheological performance of the MFC, and removal of this fraction resulted in much higher storage modulus and yield stress. Alternatively, finer fractions could be added to the MFC system to achieve a similar effect. This result

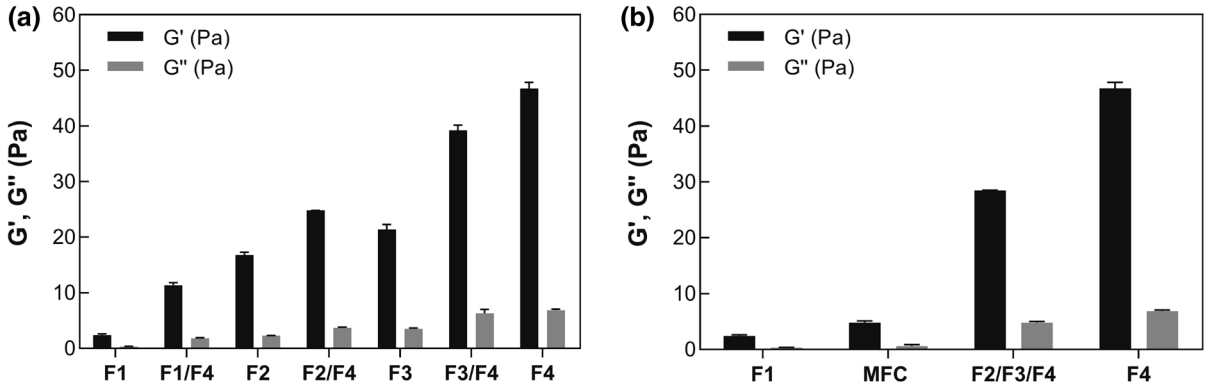

Fig. 8 Equilibrium storage and loss moduli of mixed 0.4% MFC suspensions based on different combinations of fractions, achieved by **a** addition of the finest fraction (F4) to coarser fractions or **b** removal of the coarsest fraction (F1)

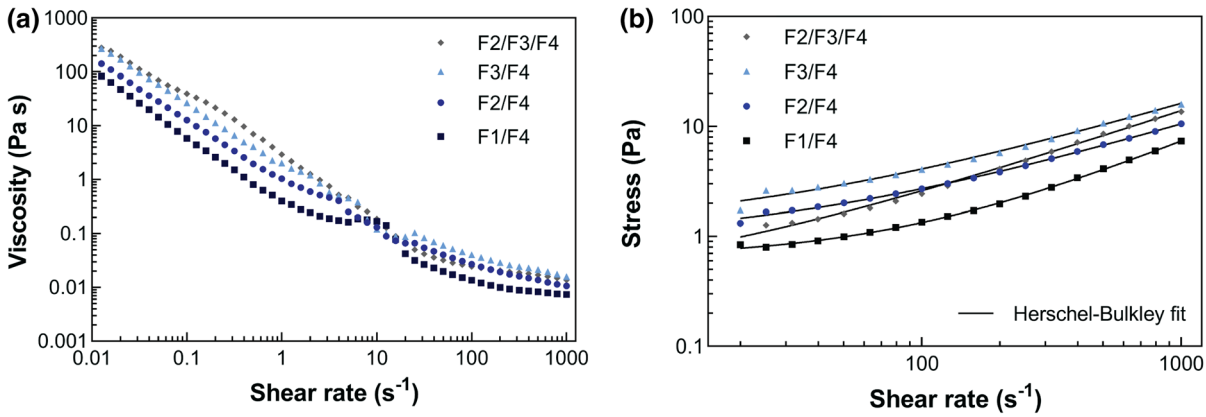

Fig. 9 Flow properties of the MFC fraction mixtures at 0.4 wt%; **a** viscosity and **b** shear stress as a function of shear rate with the Herschel–Bulkley model fits

Table 4 Yield stress and flow index of different compositions of MFC fractions based on the Herschel–Bulkley model

	Yield stress (Pa)	n	R^2
F1/F4	0.6 ± 0.1	0.9	0.99
F2/F4	0.8 ± 0.1	0.7	0.99
F3/F4	1.1 ± 0.2	0.9	0.99
F2/F3/F4	0.5 ± 0.1	0.8	0.99
MFC (unfractionated)	0.4 ± 0.1	0.8	0.99

demonstrates the possibility to systematically optimize and tailor rheological properties by mixing MFC fractions, or MFC grades, with different morphology, size, and surface charge. The significance for systematic product development is substantial and of relevance for adhesives, paints, coatings, personal care products, biocomposites, packaging, etc.

Acknowledgments This study has received funding from the Bio-Based Industries Joint Undertaking under the European Union's Horizon 2020 research and innovation programme under Grant Agreement No. 709746.

Funding Open access funding provided by Royal Institute of Technology.

References

Celzard A, Fierro V, Pizzi A (2008) Flocculation of cellulose fibre suspensions: the contribution of percolation and effective-medium theories. Cellulose 15(6):803. https://doi.org/10.1007/s10570-008-9229-1

Celzard A, Fierro V, Kerekes R (2009) Flocculation of cellulose fibres: new comparison of crowding factor with percolation and effective-medium theories. Cellulose 16(6):983–987. https://doi.org/10.1007/s10570-009-9314-0

Desmaisons J, Boutonnet E, Rueff M, Dufresne A, Bras J (2017) A new quality index for benchmarking of different cellulose nanofibrils. Carbohydr Polym 174:318–329. https://doi.org/10.1016/j.carbpol.2017.06.032

Dimic-Misic K, Gane P, Paltakari J (2013) Micro-and nanofibrillated cellulose as a rheology modifier additive in CMC-containing pigment-coating formulations. Ind Eng Chem Res 52(45):16066–16083. https://doi.org/10.1021/ie4028878

Dimic-Misic K, Maloney T, Gane P (2018) Effect of fibril length, aspect ratio and surface charge on ultralow shear-induced structuring in micro and nanofibrillated cellulose aqueous suspensions. Cellulose 25(1):117–136. https://doi.org/10.1007/s10570-017-1584-3

Fall AB, Lindström SB, Sundman O, Ödberg L, Wågberg L (2011) Colloidal stability of aqueous nanofibrillated cellulose dispersions. Langmuir 27(18):11332–11338. https://doi.org/10.1021/la201947x

Fall AB, Lindström SB, Sprakel J, Wågberg L (2013) A physical cross-linking process of cellulose nanofibril gels with shear-controlled fibril orientation. Soft Matter 9(6):1852–1863. https://doi.org/10.1039/C2SM27223G

Geng L, Mittal N, Zhan C, Ansari F, Sharma PR, Peng X, Hsiao BS, Söderberg LD (2018) Understanding the mechanistic behavior of highly charged cellulose nanofibers in aqueous systems. Macromolecules 51(4):1498–1506. https://doi.org/10.1021/acs.macromol.7b02642

Hill RJ (2008) Elastic modulus of microfibrillar cellulose gels. Biomacromol 9(10):2963–2966. https://doi.org/10.1021/bm800490x

Holtan S, Read MR, Øvrebø HH, Vold IMN (2019) Microfibrillated cellulose. US10337146B2, Jul. 2., 2019

Hon DN-S (1994) Cellulose: a random walk along its historical path. Cellulose 1(1):1–25. https://doi.org/10.1007/BF00818796

Hubbe MA, Tayeb P, Joyce M, Tyagi P, Kehoe M, Dimic-Misic K, Pal L (2017) Rheology of nanocellulose-rich aqueous suspensions: a review. BioResources 12(4):9556–9661

Isogai A (2013) Wood nanocelluloses: fundamentals and applications as new bio-based nanomaterials. J Wood Sci 59(6):449–459. https://doi.org/10.1007/s10086-013-1365-z

Kargarzadeh H, Mariano M, Gopakumar D, Ahmad I, Thomas S, Dufresne A, Huang J, Lin N (2018) Advances in cellulose nanomaterials. Cellulose 25:1–39. https://doi.org/10.1007/s10570-018-1723-5

Karppinen A, Vesterinen A-H, Saarinen T, Pietikäinen P, Seppälä J (2011) Effect of cationic polymethacrylates on the rheology and flocculation of microfibrillated cellulose. Cellulose 18(6):1381–1390. https://doi.org/10.1007/s10570-011-9597-9

Karppinen A, Saarinen T, Salmela J, Laukkanen A, Nuopponen M, Seppälä J (2012) Flocculation of microfibrillated cellulose in shear flow. Cellulose 19(6):1807–1819. https://doi.org/10.1007/s10570-012-9766-5

Kerekes R, Schell C (1992) Regimes by a crowding factor. J Pulp Pap Sci 18(1):J32–J38

Koponen AI (2020) The effect of consistency on the shear rheology of aqueous suspensions of cellulose micro-and nanofibrils: a review. Cellulose 27:1879–1897. https://doi.org/10.1007/s10570-019-02908-w

Koponen AI, Lauri J, Haavisto S, Fabritius T (2018) Rheological and flocculation analysis of microfibrillated cellulose suspension using optical coherence tomography. Appl Sci 8(5):755. https://doi.org/10.3390/app8050755

Kumar V, Nazari B, Bousfield D, Toivakka M (2016) Rheology of microfibrillated cellulose suspensions in pressure-driven flow. Appl Rheol 26(4):24–34. https://doi.org/10.3933/applrheol-26-43534

Larsson PA, Riazanova AV, Cinar Ciftci G, Rojas R, Øvrebø HH, Wågberg L, Berglund LA (2019) Towards optimised size distribution in commercial microfibrillated cellulose: a fractionation approach. Cellulose 26:1565–1575. https://doi.org/10.1007/s10570-018-2214-4

Lasseuguette E, Roux D, Nishiyama Y (2008) Rheological properties of microfibrillar suspension of TEMPO-oxidized pulp. Cellulose 15(3):425–433. https://doi.org/10.1007/s10570-007-9184-2

Lauri J, Koponen A, Haavisto S, Czajkowski J, Fabritius T (2017) Analysis of rheology and wall depletion of microfibrillated cellulose suspension using optical coherence tomography. Cellulose 24(11):4715–4728. https://doi.org/10.1007/s10570-017-1493-5

Mahrdt E, Pinkl S, Schmidberger C, van Herwijnen HW, Veigel S, Gindl-Altmutter W (2016) Effect of addition of microfibrillated cellulose to urea-formaldehyde on selected adhesive characteristics and distribution in particle board. Cellulose 23(1):571–580. https://doi.org/10.1007/s10570-015-0818-5

Mason S (1954) Fiber motions and flocculation. Tappi 37:494–501

Mendoza L, Batchelor W, Tabor RF, Garnier G (2018) Gelation mechanism of cellulose nanofibre gels: a colloids and interfacial perspective. J Colloid Interface Sci 509:39–46. https://doi.org/10.1016/j.jcis.2017.08.101

Mohtaschemi M, Sorvari A, Puisto A, Nuopponen M, Seppälä J, Alava MJ (2014) The vane method and kinetic modeling: shear rheology of nanofibrillated cellulose suspensions. Cellulose 21(6):3913–3925. https://doi.org/10.1007/s10570-014-0409-x

Mullineux G (2008) Non-linear least squares fitting of coefficients in the Herschel-Bulkley model. Appl Math Model 32(12):2538–2551. https://doi.org/10.1016/j.apm.2007.09.010

Naderi A, Lindström T, Sundström J (2014) Carboxymethylated nanofibrillated cellulose: rheological studies. Cellulose 21(3):1561–1571. https://doi.org/10.1007/s10570-014-0192-8

Nechyporchuk O, Belgacem MN, Bras J (2016a) Production of cellulose nanofibrils: a review of recent advances. Ind Crops Prod 93:2–25. https://doi.org/10.1016/j.indcrop.2016.02.016

Nechyporchuk O, Belgacem MN, Fdr Pignon (2016b) Current progress in rheology of cellulose nanofibril suspensions. Biomacromol 17(7):2311–2320. https://doi.org/10.1021/acs.biomac.6b00668

Oh K, Lee J-H, Im W, Rajabi Abhari A, Lee HL (2017) Role of cellulose nanofibrils in structure formation of pigment coating layers. Ind Eng Chem Res 56(34):9569–9577. https://doi.org/10.1021/acs.iecr.7b02750

Osong SH, Norgren S, Engstrand P (2016) Processing of wood-based microfibrillated cellulose and nanofibrillated cellulose, and applications relating to papermaking: a review. Cellulose 23(1):93–123. https://doi.org/10.1007/s10570-015-0798-5

Pääkkö M, Ankerfors M, Kosonen H, Nykänen A, Ahola S, Österberg M, Ruokolainen J, Laine J, Larsson PT, Ikkala O (2007) Enzymatic hydrolysis combined with mechanical shearing and high-pressure homogenization for nanoscale cellulose fibrils and strong gels. Biomacromol 8(6):1934–1941. https://doi.org/10.1021/bm061215p

Saito T, Uematsu T, Kimura S, Enomae T, Isogai A (2011) Self-aligned integration of native cellulose nanofibrils towards producing diverse bulk materials. Soft Matter 7(19):8804–8809. https://doi.org/10.1039/C1SM06050C

Schenker M, Schoelkopf J, Gane P, Mangin P (2018) Influence of shear rheometer measurement systems on the rheological properties of microfibrillated cellulose (MFC) suspensions. Cellulose 25(2):961–976. https://doi.org/10.1007/s10570-017-1642-x

Schenker M, Schoelkopf J, Gane P, Mangin P (2019) Rheology of microfibrillated cellulose (MFC) suspensions: influence of the degree of fibrillation and residual fibre content on flow and viscoelastic properties. Cellulose 26(2):845–860. https://doi.org/10.1007/s10570-018-2117-4

Siqueira G, Tapin-Lingua S, Bras J, da Silva Perez D, Dufresne A (2010) Morphological investigation of nanoparticles obtained from combined mechanical shearing, and enzymatic and acid hydrolysis of sisal fibers. Cellulose 17(6):1147–1158. https://doi.org/10.1007/s10570-010-9449-z

Song J, Caggioni M, Squires TM, Gilchrist JF, Prescott SW, Spicer PT (2019) Heterogeneity, suspension, and yielding in sparse microfibrous cellulose gels 1. Bubble rheometer studies. Rheol Acta 58(5):217–229. https://doi.org/10.1007/s00397-019-01140-4

Swerin A, Powell RL, Odberg L (1992) Linear and nonlinear dynamic viscoelasticity of pulp fiber suspensions. Nord Pulp Pap Res J 7(3):126–132a. https://doi.org/10.3183/npprj-1992-07-03-p126-132

Switzer LH, Klingenberg DJ (2003) Rheology of sheared flexible fiber suspensions via fiber-level simulations. J Rheol 47(3):759–778. https://doi.org/10.1122/1.1566034

Taheri H, Samyn P (2016) Effect of homogenization (microfluidization) process parameters in mechanical production of micro-and nanofibrillated cellulose on its rheological and morphological properties. Cellulose 23(2):1221–1238. https://doi.org/10.1007/s10570-016-0866-5

Tanaka R, Saito T, Hondo H, Isogai A (2015) Influence of flexibility and dimensions of nanocelluloses on the flow properties of their aqueous dispersions. Biomacromol 16(7):2127–2131. https://doi.org/10.1021/acs.biomac.5b00539

Thomas B, Raj MC, Joy J, Moores A, Drisko GL, Sanchez C (2018) Nanocellulose, a versatile green platform: from biosources to materials and their applications. Chem Rev 118(24):11575–11625. https://doi.org/10.1021/acs.chemrev.7b00627